Investigation of Surface-inset Machines with Mixed Grade Magnets Considering Magnet Thickness

Youyuan Ni, Liang Zhang, and Zhiwei Qiu

***Abstract*—This paper presents a mixed grade magnet model for surface-inset machines considering the magnet thickness. In the polar coordinates, on the basis of the Laplace/quasi-Poisson equations and boundary conditions, the constructed matrix equations are solved and the air gap magnetic field in the machine is derived. Taking an 8-pole/12-slot surface-inset motor as an example, through the presented optimization process, the air gap field is optimized considering the magnet thickness, remanence and magnetization angle. In addition, the back-EMF and electromagnetic torque are analytically obtained. The optimized results show that the proposed mixed grade magnet model has larger electromagnetic torque and smaller torque ripple than the conventional one. Finally, the analytical predictions are evaluated by finite element analysis (FEA).**

***Index Terms*—Mixed grade magnet, Surface-inset machines, Magnet thickness, Remanence, Torque ripple.**

I. Introduction

BRUSHLESS DC/AC permanent magnet (PM) machines are extensively applied in various fields because of their remarkable advantages including the simple structure, high power density and efficiency [1]–[3].

In order to reduce the magnet usage and increase the machine performance, the relatively complex magnet structures used for surface-mounted machines are proposed. A surface-mounted double-layer Halbach machine is investigated and its performance is better than the single-layer one [4]. The trapezoid magnets for surface-mounted machines are proposed and exhibit good performance in [5]–[8]. The surface-mounted machines with T-type magnets are proposed and compared in [9]–[10]. A magnet shape optimization method is proposed to reduce the harmonic of the air gap flux density in [11]. All of these various magnet shapes are used for surface-mounted machines.

Due to the robust structure, high torque density and wide field weakening region, surface-inset PM machines are also extensively used [12]. Slotless surface-inset radial/parallel magnetization machines are analytically investigated [13]–[15]. Considering the stator slotting effect, a sub-domain model method is utilized to solve the magnetic field distribution in the surface-inset machine [16]–[20]. Compared with the traditional radial/parallel magnetization, Halbach magnetized PM machine has more sinusoidal magnetic field distribution and lower torque ripple [21]. A surface-inset machine eccentric Halbach magnets is analyzed and optimized in [22]. For surface-inset multi-segment Halbach machines, general analytical optimization model is used for both odd- and even-segment Halbach magnets in [23]. However, the mixed grade magnets have not been applied for surface-inset machines yet.

In this paper, an analytical model is proposed for surface-inset machines with novel mixed grade magnets considering the magnet thickness. The influence of both the thickness and the magnet remanence on the air gap field is considered. The optimization process is presented and explained. The results show that the proposed optimized model has better performance than the conventional surface-inset Halbach machine. Finally, the analytical results are validated by finite element analysis (FEA).

II. Proposed Magnet Model

Fig. 1(a) shows the conventional surface-inset two-segment Halbach magnets. The proposed surface-inset mixed magnet structure is shown in Fig. 1(b). The magnetic pole structure is divided into the outer/inner magnets. The outer magnets are two-segment Halbach array and the inner magnet adopts parallel magnetization.

Fig. 2 shows the two-dimensional (2-D) parameters of the slotless machine with proposed mixed magnets. The parameter relation equations can be written as:

$$R_h = R_r + h_{m2} \tag{1}$$

$$R_s = R_m + g \tag{2}$$

where R_h is the outer radius of inner magnets, g is the air gap length, R_s is the stator inner radius, R_r and R_m are the outer radii of the rotor core and magnets, h_{m1} and h_{m2} are the thicknesses of the outer and inner magnets, respectively.

In addition, α_r and α_p are the magnet pole-arc to pole-pitch ratios of the outer/inner magnets, respectively, β is the symmetric magnetization angle of the outer magnets.

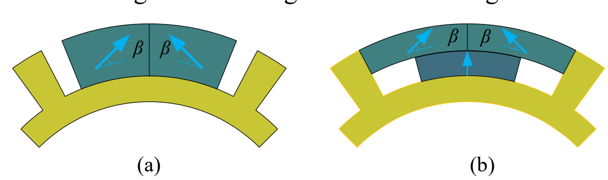

Fig. 1. Two structures of surface-inset magnets. (a) Conventional magnets. (b) Proposed mixed grade magnets.

Manuscript received April 19, 2022; revised July 6, 2022 and August 18, 2022; accepted August 23, 2022; date of publication September 25, 2022; date of current version September 18, 2022.

This work was supported by the Anhui Provincial Natural Science Foundation under Grant 2008085ME179, Anhui Province Key Laboratory of Renewable Energy Utilization and Energy Saving and the 111 Project under Grant BP0719039.*(Corresponding Author: Youyuan Ni)*

Youyuan Ni, Liang Zhang, and Zhiwei Qiu are with the School of Electrical Engineering & Automation, Hefei University of Technology, Hefei, 230009, China. (e-mail: nyy76@163.com; 2404107990@qq.com; 2641054370@qq.com).

Digital Object Identifier 10.30941/CESTEMS.2022.00035

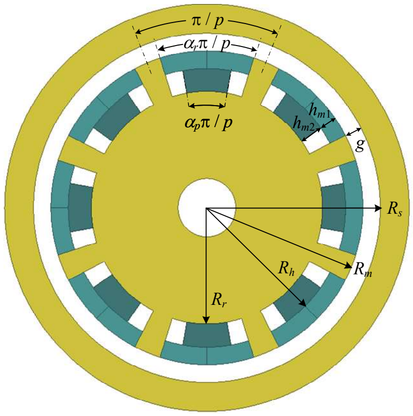

Fig. 2. Structural parameters of slotless surface-inset machine with proposed magnets.

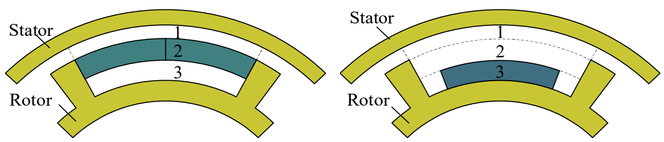

(a) (b)

Fig. 3. Solution regions of slotless machine with proposed magnets. (a) Solution regions for outer magnets. (b) Solution regions for inner magnets.

III. Solution Slotless Open-Circuit Field

Required assumptions for a 2-D model include: 1) linearly demagnetized character of magnets; 2) infinite permeability of iron; 3) neglected winding end effect.

Fig. 3 shows the regions of solution the open-circuit field in the slotless machine with proposed magnets.

A. Field Produced by Outer Magnets

As shown in Fig. 3(a), for the field produced by the outer magnets, three regions are required. Regions 1 and 3 are the air and region 2 is the magnet. In the polar coordinates, the expressions of magnetization components, M_r and M_θ, can be written as

$$M_r = \sum_{j=1,3,5\ldots}^{\infty} M_{rj}\cos(jp\theta) \tag{3}$$

$$M_\theta = \sum_{j=1,3,5\ldots}^{\infty} M_{\theta j}\sin(jp\theta) \tag{4}$$

The expressions of Fourier decomposition coefficients of M_{rj} and $M_{\theta j}$ are given in [22]. And

$$M_j = M_{rj} + jpM_{\theta j} \tag{5}$$

According to [24], the scalar magnetic potential from the general solutions of Laplace/quasi-Poisson equations in the three regions are

$$\varphi_1 = \sum_{i=1,3,5\ldots}^{\infty} (A_{i1}r^{ip} + B_{i1}r^{-ip})\cos(ip\theta) \tag{6}$$

$$\varphi_2 = \sum_{j=1,3,5\ldots}^{\infty} (A_{j2}r^{jp} + B_{j2}r^{-jp})\cos(\frac{jp\theta}{a_r}) + \sum_{j=1,3,5\ldots}^{\infty} \frac{rM_j}{\mu_r[(jp)^2-1]}\left[(\frac{R_h}{r})^{jp+1}-1\right]\cos(\frac{jp\theta}{a_r}) \tag{7}$$

$$\varphi_3 = \sum_{j=1,3,5\ldots}^{\infty} (A_{j3}r^{jp} + B_{j3}r^{-jp})\cos(jp\theta) \tag{8}$$

where i and j are harmonic orders, A_{i1}, B_{i1}, A_{j1}, B_{j1}, A_{j2} and B_{j2} are coefficients to be solved, p is the number of pole-pairs, μ_0 is the air permeability, and θ is the rotor position angle.

In the air and magnet regions, the relation equations between the two magnetic field vectors (i.e., the flux density B and the field intensity H) are given in [13].

Along the stator bore, the boundary condition is

$$H_{\theta 1}\big|_{r=R_s} = 0 \tag{9}$$

According to (6), the field components in region 1, $H_{\theta 1}$ and B_{r1}, can be obtained as

$$H_{\theta 1} = \sum_{i=1,3,5\ldots}^{\infty} A_{i1}\left[ipr^{ip-1} - \frac{R_s^{\,2ip}}{r^{ip+1}}\right]\sin(ip\theta) \tag{10}$$

$$B_{r1} = -\mu_0 \sum_{i=1,3,5\ldots}^{\infty} A_{i1}ip\left[r^{ip-1} + \frac{R_s^{\,2ip}}{r^{ip+1}}\right]\cos(ip\theta) \tag{11}$$

For regions 2 and 3, the boundary conditions are

$$H_{\theta 3}\big|_{r=R_r} = 0 \tag{12}$$

$$H_{\theta 2}\big|_{r=R_h} = H_{\theta 3}\big|_{r=R_h} \tag{13}$$

$$B_{r2}\big|_{r=R_h} = B_{r3}\big|_{r=R_h} \tag{14}$$

Thus, according to (7)–(8) and (12)–(14), the field components in regions 2 and 3 can be written as

$$H_{\theta 2} = \sum_{j=1,3,5\ldots}^{\infty} \left[A_{j2}r^{jp} + rP_1 + Q_1\right]\frac{jp}{\alpha_r r}\sin(\frac{jp\theta}{\alpha_r}) \tag{15}$$

$$B_{r2} = -\mu_0\mu_r \sum_{j=1,3,5\ldots}^{\infty} \cos(\frac{jp\theta}{\alpha_r})(A_{j2}jpr^{jp-1} + P_2 - Q_2) + \mu_0 M_r \tag{16}$$

$$H_{\theta 3} = \sum_{j=1,3,5\ldots}^{\infty} A_{j3}(r^{jp-1} - \frac{R_r^{\,2jp}}{r^{jp+1}})\frac{jp}{\alpha_r}\sin(\frac{jp\theta}{\alpha_r}) \tag{17}$$

$$B_{r3} = -\mu_0 \sum_{j=1,3,5\ldots}^{\infty} jpA_{j3}(r^{jp-1} + \frac{R_r^{\,2jp}}{r^{jp+1}})\cos(\frac{jp\theta}{\alpha_r}) \tag{18}$$

where

$$\begin{cases} P_1 = \dfrac{M_{rj} + jpM_{\theta j}}{\mu_r(j_2p^2-1)}\left[(\dfrac{R_h}{r})^{jp+1} - 1\right] \\ P_2 = -\dfrac{M_{rj} + jpM_{\theta j}}{\mu_r(j_2p^2-1)}\left[jp(\dfrac{R_h}{r})^{jp+1} + 1\right] \end{cases} \tag{19}$$

$$\begin{cases} Q_1 = \dfrac{I_1 + I_2 + \ldots\ldots + I_7}{jp(jp-1)r^{jp}I_8} \\ Q_2 = \dfrac{I_1 + I_2 + \ldots\ldots + I_7}{(jp-1)r^{jp}I_8} \end{cases} \tag{20}$$

where

$$\begin{cases} I_1 = M_r R_h^{\,jp}(1-jp) \\ I_2 = -(M_{rj} + jpM_{\theta j})R_h^{\,jp}\cos(\dfrac{jp\theta}{\alpha_r}) \end{cases} \tag{21}$$

$$\begin{cases} I_3 = (M_{rj} + jpM_{\theta j})\dfrac{R_r^{2jp}}{R_h^{jp}}\cos(\dfrac{jp\theta}{\alpha_r}) \\ I_4 = M_r R_r^{2jp}(jp-1) \end{cases} \tag{22}$$

$$\begin{cases} I_5 = A_{j2} R_h^{2jp-1}(1-jp)jp\cos(\dfrac{jp\theta}{\alpha_r}) \\ I_6 = A_{j2}\dfrac{R_r^{2jp}jp(1-jp)(1+\mu_r)}{R_h}\cos(\dfrac{jp\theta}{\alpha_r}) \end{cases} \tag{23}$$

$$\begin{cases} I_7 = A_{j2} R_h^{2jp-1}\mu_r jp(jp-1)\cos(\dfrac{jp\theta}{\alpha_r}) \\ I_8 = \dfrac{(1+\mu_r)R_h^{2jp} + (1-\mu_r)R_r^{2jp}}{R_h^{2jp+1}}\cos(\dfrac{jp\theta}{\alpha_r}) \end{cases} \tag{24}$$

Thus, only two coefficients A_{i1} and A_{j1} are to be determined. The interface conditions for regions 1 and 2 are

$$H_{\theta 1}\big|_{r=R_m} = H_{\theta 2}\big|_{r=R_m} \tag{25}$$

$$B_{r1}\big|_{r=R_m} = B_{r2}\big|_{r=R_m} \tag{26}$$

The integral equations can be written as

$$\int_{-\frac{\pi}{2p}}^{\frac{\pi}{2p}} H_{\theta 1}\sin(ip\theta)d\theta = \int_{-\frac{\alpha_r\pi}{2p}}^{\frac{\alpha_r\pi}{2p}} H_{\theta 2}\sin(ip\theta)d\theta \tag{27}$$

$$\int_{-\frac{\alpha_r\pi}{2p}}^{\frac{\alpha_r\pi}{2p}} B_{r1}\cos(\frac{jp\theta}{\alpha_r})d\theta = \int_{-\frac{\alpha_r\pi}{2p}}^{\frac{\alpha_r\pi}{2p}} B_{r2}\cos(\frac{jp\theta}{\alpha_r})d\theta \tag{28}$$

From (27) and (28), the matrix equation is written as

$$\begin{pmatrix} \mathbf{A}_{ii} & \mathbf{B}_{ij} \\ \mathbf{C}_{ji} & \mathbf{D}_{jj} \end{pmatrix}\begin{pmatrix} \mathbf{A}_1 \\ \mathbf{A}_2 \end{pmatrix} = \begin{pmatrix} \mathbf{E}_i \\ \mathbf{F}_j \end{pmatrix} \tag{29}$$

where $\mathbf{A}_{ii}$, $\mathbf{B}_{ij}$, $\mathbf{C}_{ji}$, $\mathbf{D}_{jj}$, $\mathbf{E}_i$, and $\mathbf{F}_j$ are given matrixs, the column matrices $\mathbf{A}_1$ and $\mathbf{A}_2$ can be expressed as

$$\mathbf{A}_1 = \begin{pmatrix} A_{11} \\ A_{21} \\ \cdots \\ A_{i1} \end{pmatrix},\ \mathbf{A}_2 = \begin{pmatrix} A_{12} \\ A_{22} \\ \cdots \\ A_{j2} \end{pmatrix} \tag{30}$$

Therefore, the field produced by the outer magnets can be obtained by solving (29).

B. Field Produced by Inner Magnets

The inner magnets are parallel magnetized, and the magnetization components, M'_r and M'_θ, are given in [22].

The solution subdomains for the inner magnets is shown in Fig. 3(b). Similarly, the scalar magnetic potentials φ'_1, φ'_2 and φ'_3 in the three subdomains can be obtained from Laplace/quasi-Poisson equations.

The boundary conditions are

$$H'_{\theta 1}\big|_{r=R_s} = 0 \tag{31}$$

$$H'_{\theta 3}\big|_{r=R_r} = 0 \tag{32}$$

$$\begin{cases} H'_{\theta 1}\big|_{r=R_m} = H'_{\theta 2}\big|_{r=R_m} \\ B'_{r1}\big|_{r=R_m} = B'_{r2}\big|_{r=R_m} \end{cases} \tag{33}$$

$$\begin{cases} H'_{\theta 2}\big|_{r=R_h} = H'_{\theta 3}\big|_{r=R_h} \\ B'_{r2}\big|_{r=R_h} = B'_{r3}\big|_{r=R_h} \end{cases} \tag{34}$$

According to (31)–(40), the field components in regions 1 and 2 can be obtained as

$$H'_{\theta 1} = \sum_{i=1,3,5\ldots}^{\infty} A'_{i1}\left[ipr^{ip-1} - \frac{R_s^{2ip}}{r^{ip+1}}\right]\sin(ip\theta) \tag{35}$$

$$B'_{r1} = -\mu_0\sum_{j=1,3,5\ldots}^{\infty} A'_{i1}ip\left[r^{ip-1} + \frac{R_s^{2ip}}{r^{ip+1}}\right]\cos(ip\theta) \tag{36}$$

$$H'_{\theta 2} = \sum_{i=1,3,5\ldots}^{\infty}\frac{jp}{\alpha_r r}(A'_{j2}r^{jp} + Q')\sin(\frac{jp\theta}{\alpha_r}) \tag{37}$$

$$B'_{\theta 2} = -\mu_0\sum_{j=1,3,5\ldots}^{\infty} jp(A'_{j2}r^{jp-1} - \frac{Q'}{r^{jp}})\cos(\frac{jp\theta}{\alpha_r}) \tag{38}$$

where Q' is the known coefficient obtained by the boundary conditions, A'_{i1} and A'_{j2} are the unknown coefficients to be solved.

According to (33) and (34)–(38), the integral equations can be given as

$$\int_{-\frac{\pi}{2p}}^{\frac{\pi}{2p}} H'_{\theta 1}\sin(ip\theta)d\theta = \int_{-\frac{\alpha_r\pi}{2p}}^{\frac{\alpha_r\pi}{2p}} H'_{\theta 2}\sin(ip\theta)d\theta \tag{39}$$

$$\int_{-\frac{\alpha_r\pi}{2p}}^{\frac{\alpha_r\pi}{2p}} B'_{r1}\cos(\frac{jp\theta}{\alpha_r})d\theta = \int_{-\frac{\alpha_r\pi}{2p}}^{\frac{\alpha_r\pi}{2p}} B'_{r2}\cos(\frac{jp\theta}{\alpha_r})d\theta \tag{40}$$

From (39) and (40), the matrix equation is written as

$$\begin{pmatrix} \mathbf{A}'_{ii} & \mathbf{B}'_{ij} \\ \mathbf{C}'_{ji} & \mathbf{D}'_{jj} \end{pmatrix}\begin{pmatrix} \mathbf{A}'_1 \\ \mathbf{A}'_2 \end{pmatrix} = \begin{pmatrix} \mathbf{E}'_i \\ \mathbf{F}'_j \end{pmatrix} \tag{41}$$

where A'_{ii}, $\mathbf{B}'_{ij}$, $\mathbf{C}'_{ji}$, $\mathbf{D}'_{jj}$, $\mathbf{E}'_i$, and $\mathbf{F}'_j$ are known matrixs, the column matrices $\mathbf{A}_1$ and $\mathbf{A}_2$ can be expressed as

$$\mathbf{A}'_1 = \begin{pmatrix} A'_{11} \\ A'_{21} \\ \cdots \\ A'_{i1} \end{pmatrix},\ \mathbf{A}'_2 = \begin{pmatrix} A'_{12} \\ A'_{22} \\ \cdots \\ A'_{j2} \end{pmatrix} \tag{42}$$

Therefore, the field produced by the inner magnets can be obtained from (41).

IV. Analytical Performance of Slotted Model

A. Air Gap Field of Slotted Model

Based on a linear superposition method, the radial air gap field in the slotless machine with proposed magnets can be obtained as

$$B_{r\text{-slotless}} = B_{r1} + B'_{r1} \tag{43}$$

For the slotted machine having the parallel teeth, the air gap flux density can be written as

$$B_{r\text{-slotted}} = C \times B_{r\text{-slotless}} \tag{44}$$

where C is the Carter's coefficient in terms of the stator slot, and its detailed expression is given in [4].

B. Back-EMF

For one stator coil with N_c turns, the flux linkage can be expressed as

$$\Psi = R_s L_s N_c \int_{\omega_r t}^{\omega_r t+\alpha_{cp}} B_{r\text{-slotted}}(R_s,\theta)d\theta \tag{45}$$

where ω_r is the angular frequency, L_s is the coil active length, and α_{cp} is the coil pitch angle.

Then, the back-EMF can be obtained as

$$E = -\frac{d\Psi}{dt} = 2R_s L_s N_c \sum_{n=1,3,5\ldots}^{\infty} B_{r\text{-slotted}} \sin(\frac{np\pi}{N_s})\sin(np\omega_r t) \tag{46}$$

where N_s is the slot number.

For an 8-pole/12-slot machine, each phase winding has four coils. The induced electromotive forces of all coils are

$$\begin{cases} E_{a1} = 2R_s L_s N_c \sum\limits_{n=1,3,5\ldots}^{\infty} B_{r\text{-slotted}} \sin(\frac{np\pi}{N_s})\sin(np\omega_r t) \\ E_{a2} = 2R_s L_s N_c \sum\limits_{n=1,3,5\ldots}^{\infty} B_{r\text{-slotted}} \sin(\frac{np\pi}{N_s})\sin(np\omega_r t-\frac{6\pi}{N_s}) \\ E_{a3} = 2R_s L_s N_c \sum\limits_{n=1,3,5\ldots}^{\infty} B_{r\text{-slotted}} \sin(\frac{np\pi}{N_s})\sin(np\omega_r t-\frac{12\pi}{N_s}) \\ E_{a4} = 2R_s L_s N_c \sum\limits_{n=1,3,5\ldots}^{\infty} B_{r\text{-slotted}} \sin(\frac{np\pi}{N_s})\sin(np\omega_r t-\frac{18\pi}{N_s}) \end{cases} \tag{47}$$

Therefore, the back-EMF of phase A is

$$E_A = E_{a1} + E_{a2} + E_{a3} + E_{a4} \tag{48}$$

The back-EMF of phases B and C can be obtained similarly.

C. Electromagnetic Torque

For a three-phase machine, the electromagnetic torque can be given as

$$T_{em} = (E_A I_A + E_B I_A + E_C I_C)/\omega_r \tag{49}$$

where I_A, I_B and I_C are three-phase balanced currents.

V. Analytical Optimization and Verification

For comparion, the usage and the average remanence per unit volume of magnets are constant, i.e.,

$$\begin{cases} S = S_o + S_i \\ B_r = (S_o B_{re1} + S_i B_{re2})/S \end{cases} \tag{50}$$

where S_o and S_i are the areas of the outer/inner magnets, respectively, B_{re1} and B_{re2} are the remanences of the outer/inner magnets, respectively. And

$$\begin{cases} S_o = a_r\pi[R_m{}^2 - (R_r + h_{m2})^2]/(2p) \\ S_i = a_r\pi[(R_r + h_{m2})^2 - R_r{}^2]/(2p) \end{cases} \tag{51}$$

According to (50) and (51), h_{m1} and B_{re1} can be represented by h_{m2} and B_{re2}. The fundamental components of air gap magnetic density B_{rf} are the function of h_{m2}, B_{re2} and β, i.e.,

$$B_{rf} = f\left(h_{m2}, B_{re2}, \beta\right) \tag{52}$$

The objective function and the constraint conditions of the optimization variables can be written as

$$\begin{cases} \max\{B_{rf}(h_{m2}, B_{re2}, \beta)\} \\ \text{Subject to.} \begin{cases} 0 < h_{m2} < 4\text{mm} \\ 1\text{T} \le B_{re2} \le 1.4\text{T} \\ 0° < \beta < 90° \end{cases} \end{cases} \tag{53}$$

If the magnet thickness is fixed, since the outer magnets have a changerable magnetization angle, the optimal value can be obtained by

$$\frac{\partial B_{r1}}{\partial \beta} = 0 \tag{54}$$

Based on the aforementioned analysis equations, 8-pole/12-slot machines with proposed mixed magnets are analyzed. The main parameters are shown in Table I.

TABLE I
Design Parameters of 8-Pole/12-Slot Machines

Item	Value	Unit
Rated speed	2000	r/min
Rated phase current	7.7	A
Stator outer radius, R_{so}	60	mm
Stator inner radius, R_s	35	mm
Magnet inner radius, R_r	30	mm
Total thickness of magnets, h	4	mm
Active length, L_s	40	mm
Magnet-arc ratio of outer magnets, α_r	0.78	
Number of coil turns, N_c	53	
Average remanence per unit volume, B_r	1.2	T
Magnet relative permeability, μ_r	1.05	

The optimization process is relatively complex, and the flow chart is presented, as shown in Fig. 4. B_{rf0} is the fundamental amplitude of air gap flux density when the inner /outer magnets are of equal thickness and the magnetization angle and remanence are both optimal. Firstly, the thickness of the inner/outer magnets are given and n is the number of combinations of the inner/outer magnets with different thicknesses. According to (54), the corresponding optimal magnetization angle β can be derived. Secondly, the influence of the remanence on the fundamental magnetic density B_{rf} is considered. Considering different inner magnet thicknesses with different optimal magnetization angles, the variation of fundamental magnetic density with the remanence of inner magnets is presented, as shown in Fig. 5. It should be noted that the dotted line in this figure are unrealistic points. It can be seen that the fundamental flux density changes monotonically with the increase of B_{re2} independent of inner magnet thickness. Thirdly, the relatively optimal h_{m2} (i.e., 2.6 mm) can be selected in Fig. 5. According to (54), β is derived as 70.5°. With derived these two parameters, the influence of the inner magnet remanence on the fundamental flux density is shown in Fig. 6. If B_{re2} is equal to 1.06 T, the maximum fundamental amplitude and minimum total harmonic distortion (THD) are determined. Thus, the relatively optimal parameters are derived as: β=70.5°, h_{m1}=1.4 mm, h_{m2}=2.6 mm, B_{re1}=1.4 T and B_{re2}=1.06 T. Finally, the optimal back-EMF and electromagnetic torque can be obtained.

It can be seen from Fig. 5 that within the available range, when h_{m2}=2.6 mm, the fundamental amplitude of the air gap magnetic density is relatively large, so h_{m2}=2.6 mm is selected as the optimal thickness of the inner magnets.

Fig. 6 shows the variation trend of the fundamental amplitude and THD of the air gap magnetic density with the remanence of the inner magnets when h_{m2}=2.6 mm. When B_{re2}=1.06 T, there is the maximum fundamental amplitude and

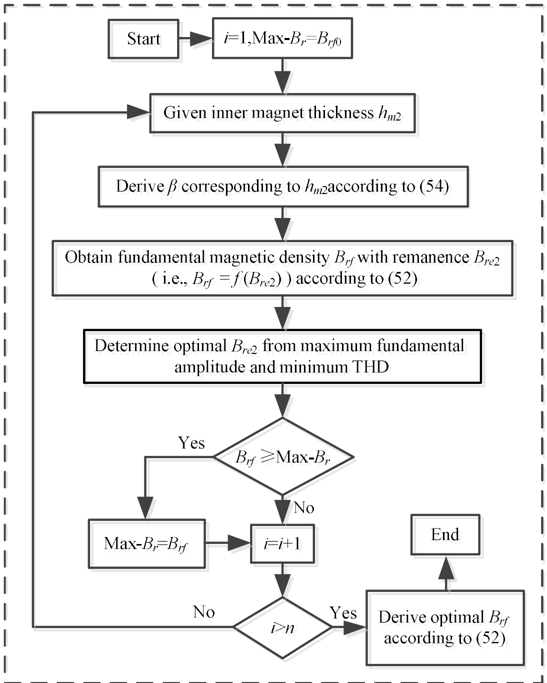

Fig. 4. Flow chart of optimization of magnet parameters.

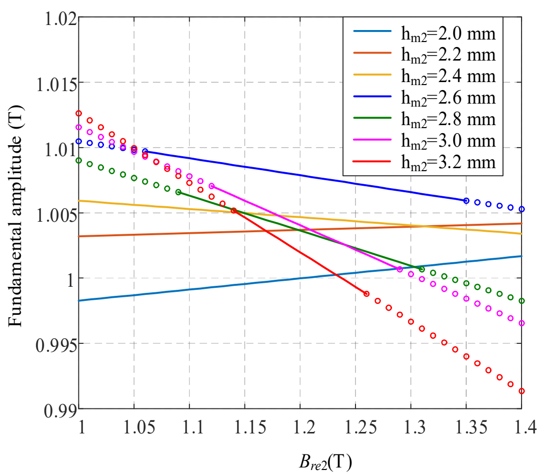

Fig. 5. Variation of fundamental amplitude of air gap magnetic density with remanence of inner magnets considering different inner magnet thickneses.

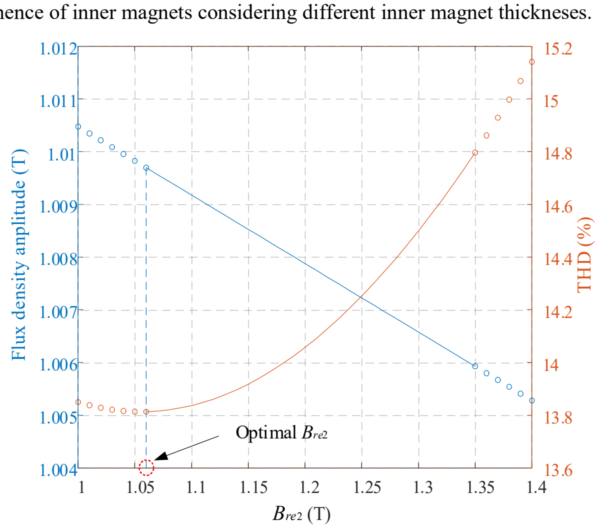

Fig. 6. Influence of inner magnet remanence on fundamental amplitude and THD of air gap field.

the minimum THD of the air gap magnetic density, as marked in Fig. 6, so B_{re2}=1.06 T is selected as the optimal remanence of the inner magnets.

The changes of the fundamental amplitude and THD of magnetic flux intensity with the magnetization angle of the outer magnets and the remanence of the inner magnets are shown in Fig. 7(a) and 7(b), respectively. It can be observed the maximum fundamental amplitude and minimum THD derived in Fig. 6 are in good agreement with those in Fig. 7.

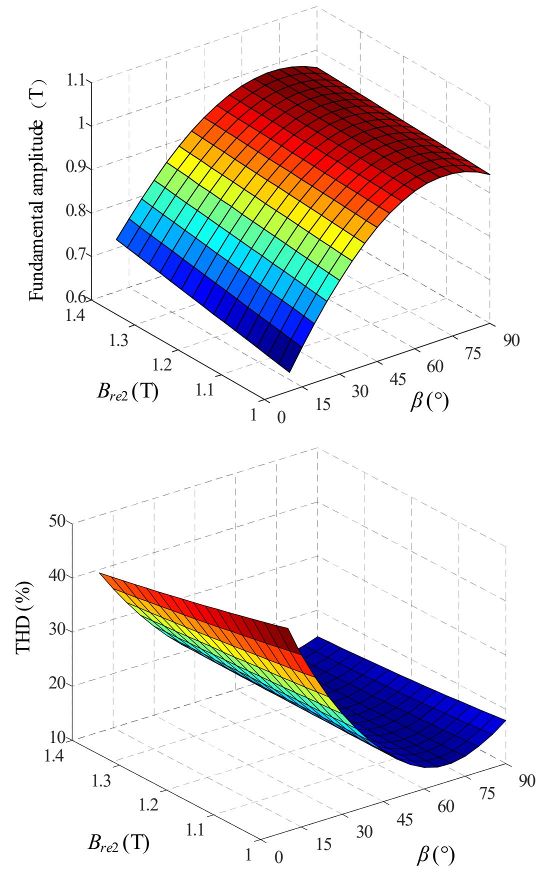

Fig. 7. Variation of fundamental amplitude and THD of air gap flux density with remanence of inner magnets and magnetization angle of outer magnets. (a) Variation of fundamental amplitude. (b) Variation of THD.

Fig. 8 shows the air gap flux density waveforms and their harmonics of the conventional/proposed machines with optimi-

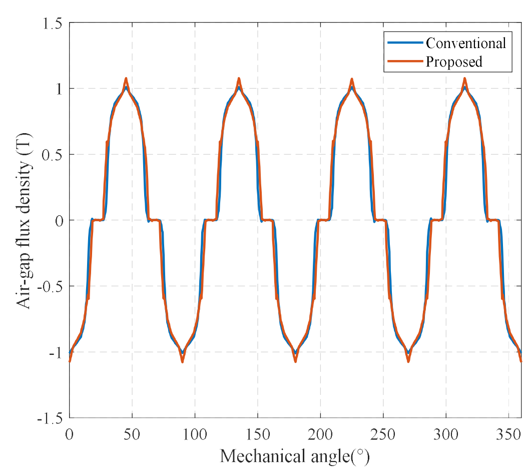

(a)

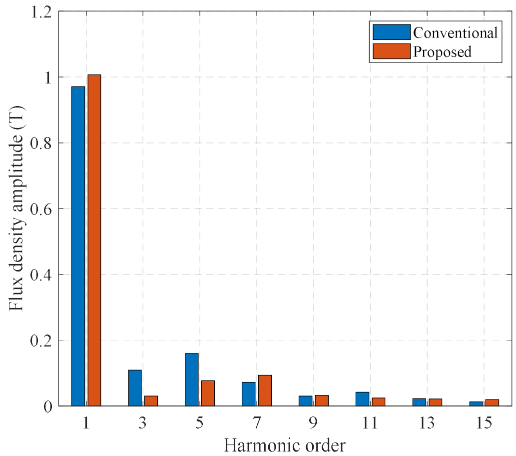

(b)

Fig. 8. Waveform/harmonic comparison of air gap magnetic density between two slotless machines. (a) Waveform comparison. (b) Harmonic comparison.

zed magnets. The optimal magnetization angle for the conventional magnet is derived as 79.5°. It can be seen from Fig. 8(b) that the air gap flux density waveforms in both two machines have no even harmonics. The proposed machine has a larger fundamental amplitude, and the 3rd and 5th harmonics are significantly smaller than those of the conventional machine.

Fig. 9 shows the back-EMF waveforms and their harmonics of the conventional/proposed machines with optimized magnets machine. Similarly, the back-EMF waveforms of both two machines have no even harmonics. Obviously, compared with conventional machine, the proposed machine model with optimized magnets has a larger fundamental component and smaller THD.

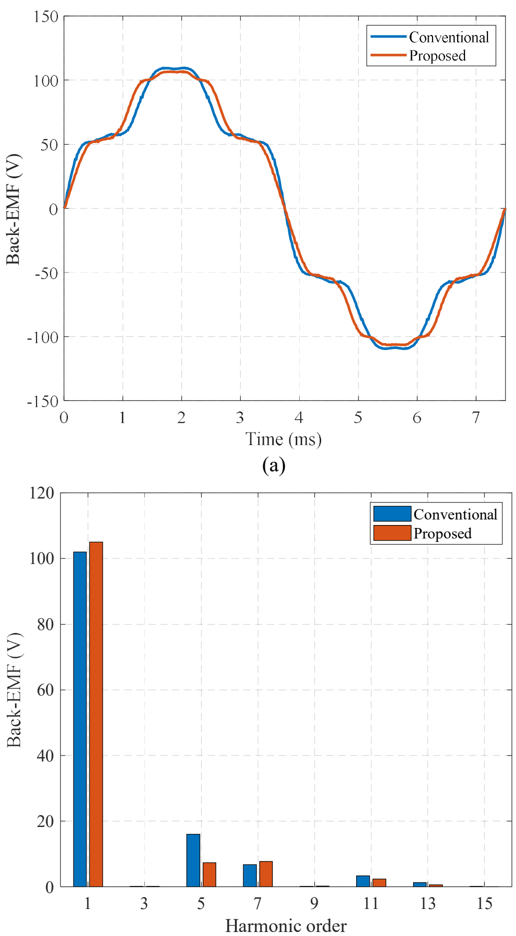

(b)

Fig. 9. Waveform/harmonic comparison of back-EMFs between two machines. (a) Waveform comparison. (b) Harmonic comparison.

Fig. 10 presents the comparison of electromagnetic torque waveforms of two different machines. Obviously, the machine with optimized combined magnets has a higher average torque and a lower torque ripple, this is mainly because the magnetic field waveform of the proposed machine model has larger fundamental and smaller harmonic components.

Fig. 11 shows the magnetic line of force distributions in machines with conventional/proposed optimized magnets by a FEA technique. The optimal magnetization angles are 79.5° and 70.5°, respectively, which are in good agreement with those from analytical method. It can be observed that the magnetic leakage occurs at the space between the magnets and rotor salient iron for both two structures. It can be also observed that the magnetic leakage in the proposed machine reduces significantly.

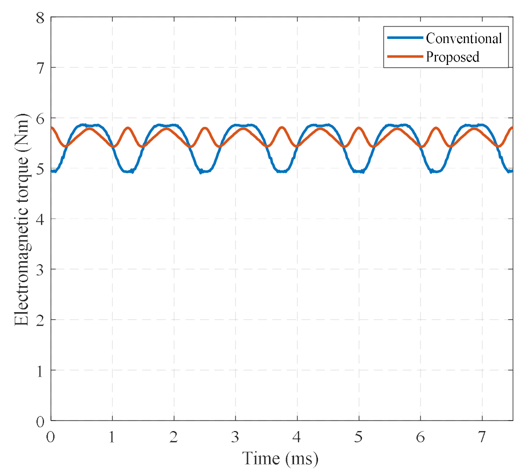

Fig. 10. Electromagnetic torque waveform comparison between two machines.

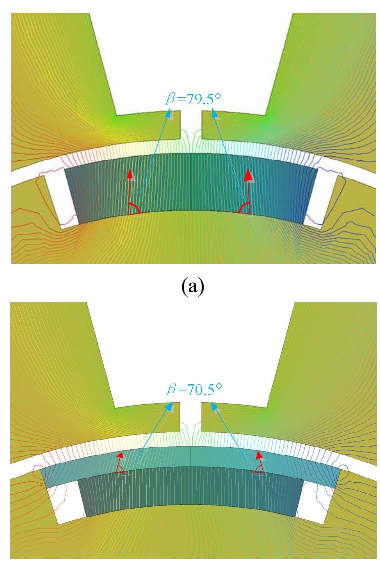

(b)

Fig. 11. Magnetic line of force distributions in machines with conventional/proposed optimized magnets. (a) Conventional. (b) Proposed.

Fig. 12 shows the magnetic force of the magnets of the conventional machine. It can be seen that the average force of the magnets is 23.82 N. Fig. 13 shows the magnetic force of the outer/inner magnets of the proposed machine. It can be observed that the average forces of the outer/inner magnets are 17.35 and 30.68 N, respectively. Although the total force of the proposed machine is larger than the counterpart of the conventional machine, the force ripple of the proposed machine is much less than the counterpart of the conventional machine.

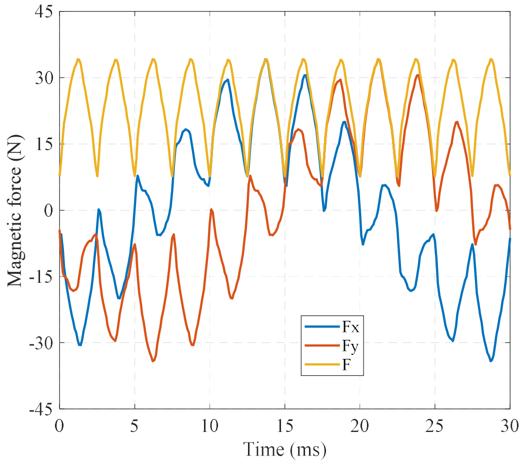

Fig. 12. Magnetic force of magnets of conventional machine.

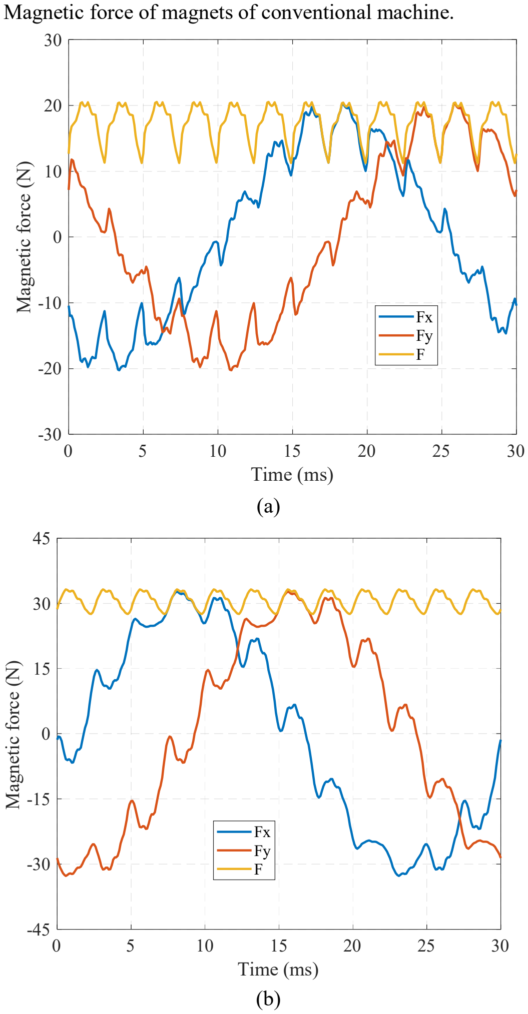

Fig. 13. Magnetic force of outer/inner magnets of proposed machine. (a) Outer magnets. (b) Inner magnets.

For the proposed optimized model, the analytical and FEA predictions of air-gap flux density, back-EMF and electromagnetic torque waveforms are shown in Fig. 14. FEA predictions verify the correctness of the analytical model. Table II lists the given/optimized magnet parameter comparison between conventional and proposed machines. Table III lists the optimized electromagnetic performance comparison between the two machines. Compared with the traditional machine, the fundamental amplitudes of the air gap flux density

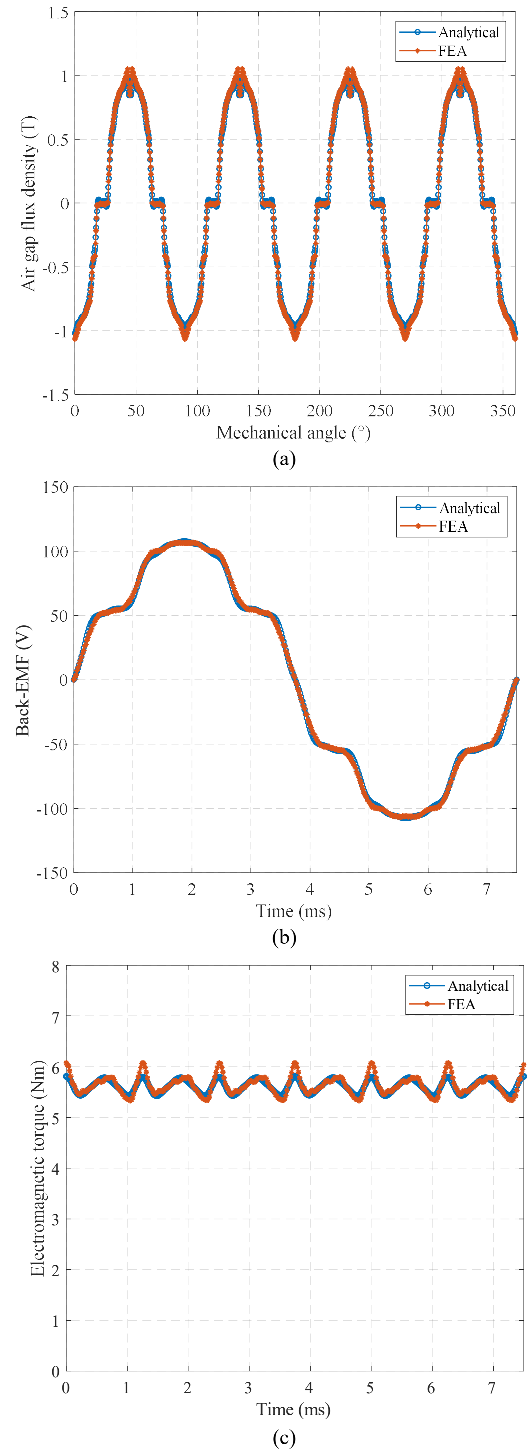

Fig. 14. Analytical and FEA predictions of waveforms of 8-pole/12-slot machine with proposed magnets. (a) Air gap flux density waveforms. (b) Back-EMF waveforms. (c) Electromagnetic torque waveforms.

and back-EMF of the proposed machine increase by 4.12% and 2.63%, respectively, and the average value of the electromagnetic torque increases by 2.36%. At the same time, the THD values of the air gap flux density and back-EMF of the proposed machine reduce by 37.1% and 39.76%, respectively, and the torque ripple reduces by 57.83%. Furthermore, due to the increase of the average value of electromagnetic torque, the efficiency of the proposed machine is also improved.

TABLE II
COMPARISON OF MAGNET PARAMETERS BETWEEN TWO MACHINES

	Conventional	Proposed
Optimized magnetization angle (°)	79.5	70.5
Given/optimized magnet thickness (mm)	4	h_{m1}=1.4 h_{m2}=2.6
Given/optimized magnet remanence (T)	1.2	B_{re1}=1.4 B_{re2}=1.06

TABLE III
COMPARISON OF OPTIMIZED PERFORMANCE BETWEEN TWO MACHINES

		Conventional	Proposed
Slotless flux density	Fundamental amplitude (T)	0.97	1.01
	THD (%)	22.27	14.03
Back-EMF	Fundamental amplitude (V)	102.52	105.22
	THD (%)	17.43	10.50
Electromagnetic torque	Average value (Nm)	5.48	5.61
	Ripple value (%)	16.22	6.84
Current density	Rated value (A/mm^2)	5.96	5.96
Efficiency	Rated value (%)	94.73	94.84

VI. CONCLUSION

A surface-inset machine model with mixed grade magnets has been presented. For this model, the scalar magnetic potential can be used to implement the analytical optimization easily and quickly. Through the subdomain model analysis and a linear superposition method, the magnetic field produced by all the magnets can be solved. Considering the magnetization angle, the thickness and the remanence of magnets, the optimization process is proposed and the optimization results are presented. It is shown that the electromagnetic performance of the proposed magnet model is better than that of the conventional magnet model. The correctness of the analytical results is verified by FEA.

REFERENCES

[1] T. Ishikawa, Y. Seki and N. Kurita, "Analysis for fault detection of vector-controlled permanent magnet synchronous motor with permanent magnet defect," *IEEE Trans. Magn.*, vol. 49, no. 5, pp. 2331-2334, May. 2013.

[2] K. Yoon and B. Kwon, "Optimal design of a new interior permanent magnet motor using a flared-shape arrangement of ferrite magnets," *IEEE Trans. Magn.*, vol. 52, no. 7, pp. 1-4, July 2016.

[3] W. Tong, S. Li, X. Pan, S. Wu and R. Tang, "Analytical model for cogging torque calculation in surface-mounted permanent magnet motors with rotor eccentricity and magnet defects," *IEEE Trans. Energy Convers.*, vol. 35, no. 4, pp. 2191-2200, Dec. 2020.

[4] Y. Ni, X. Jiang, B. Xiao and Q. Wang, "Analytical modeling and optimization of dual-layer segmented Halbach permanent-magnet Machines," *IEEE Trans. Magn.*, vol. 56, no. 5, pp. 1-11, May 2020.

[5] X. Zhang, C. Zhang, J. Yu, P. Du and L. Li, "Analytical model of magnetic field of a permanent magnet synchronous motor with a trapezoidal Halbach permanent magnet array," *IEEE Trans. Magn.*, vol. 55, no. 7, pp. 1-5, July 2019.

[6] I. I. Abdalla, T. Ibrahim and N. M. Nor, "Analysis of tubular linear motors for different shapes of magnets," *IEEE Access*, vol. 6, pp. 10297-10310, 2018.

[7] P. Liang, F. Chai, Y. Yu and L. Chen, "Analytical model of a spoke-type permanent magnet synchronous in-wheel motor with trapezoid magnet accounting for tooth saturation," *IEEE Trans. Ind. Electron.*, vol. 66, no. 2, pp. 1162-1171, Feb. 2019.

[8] K. J. Meessen, B. L. J. Gysen, J. J. H. Paulides and E. A. Lomonova, "Halbach permanent magnet shape selection for slotless tubular actuators," *IEEE Trans. Magn.*, vol. 44, no. 11, pp. 4305-4308, Nov. 2008.

[9] Y. Shen and Z. Q. Zhu, "Investigation of permanent magnet brushless machines having unequal-magnet height pole," *IEEE Trans. Magn.*,vol. 48, no. 12, pp. 4815-4830, Dec. 2012.

[10] Y. Shen and Z. Q. Zhu, "Analysis of electromagnetic performance of Halbach PM brushless machines having mixed grade and unequal height of magnets," *IEEE Trans. Magn.*,vol. 49, no. 4, pp. 1461-1469, April 2013.

[11] C. Liu, Y. Xu, J. Zou, G. Yu and L. Zhuo, "Permanent magnet shape optimization method for PMSM air gap flux density harmonics reduction," *CES Transactions on Electrical Machines and Systems*, vol. 5, no. 4, pp. 284-290, Dec. 2021.

[12] A. Rahideh and T. Korakianitis, "Analytical magnetic field distribution of slotless brushless machines with inset permanent magnets," *IEEE Trans. Magn.*, vol. 47, no. 6, pp. 1763-1774, June 2011.

[13] Z. Q. Zhu, D. Howe and Z. P. Xia, "Prediction of open-circuit airgap field distribution in brushless machines having an inset permanent magnet rotor topology," *IEEE Trans. Magn.*, vol. 30, no. 1, pp. 98-107, Jan. 1994.

[14] A. Rahideh, M. Mardaneh and T. Korakianitis, "Analytical 2-D calculations of torque, inductance, and back-EMF for brushless slotless machines with surface inset magnets," *IEEE Trans. Magn.*, vol. 49, no. 8, pp. 4873-4884, Aug. 2013.

[15] F. Dubas and A. Rahideh, "Two-dimensional analytical permanent-magnet eddy-current loss calculations in slotless PMSM equipped with surface-inset magnets," *IEEE Trans. Magn.*, vol. 50, no. 3, pp. 54-73, March 2014.

[16] F. Chen, C. Zhang, J. Chen and G. Yang, "Accurate subdomain model for computing magnetic field of short moving-magnet linear motor with Halbach array," *IEEE Trans. Magn.*, vol. 56, no. 9, pp. 1-9, Sept. 2020.

[17] Z. Zhang, C. Xia, H. Wang and T. Shi, "Analytical field calculation and analysis of surface inset permanent magnet machines with high saliency ratio," *IEEE Trans. Magn.*, vol. 52, no. 12, pp. 1-12, Dec. 2016.

[18] A. Rahideh and T. Korakianitis, "Analytical magnetic field calculation of slotted brushless permanent-magnet machines with surface inset magnets," *IEEE Trans. Magn.*, vol. 48, no. 10, pp. 2633-2649, Oct. 2012.

[19] T. Lubin, S. Mezani and A. Rezzoug, "Two-dimensional analytical calculation of magnetic field and electromagnetic torque for surface-inset permanent-magnet motors," *IEEE Trans. Magn.*, vol. 48, no. 6, pp. 2080-2091, June 2012.

[20] L. Jian, K. T. Chau, Y. Gong, C. Yu and W. Li, "Analytical calculation of magnetic field in surface-inset permanent magnet motors," *IEEE Trans. Magn.*, vol. 45, no. 10, pp. 4688-4691, Oct. 2009.

[21] Z. Q. Zhu and D. Howe, “Halbach permanent magnet machines and applications: A review,” *Proc. Inst. Elect. Eng.—Elect. Power Appl*., vol. 148, no. 4, pp. 299–308, Jul. 2001.

[22] Y. Ni, K. Chen, B. Xiao, W. Qian and Q. Wang, "Analytical modeling of PM electrical machines with eccentric surface-inset Halbach magnets," *IEEE Trans. Magn.*, vol. 57, no. 4, pp. 1-9, April 2021.

[23] Y. Ni, W. Qian, Q. Chen, K. Chen and Q. Wang, "General analytical optimization model of surface-inset electrical machines with even-/odd-segment Halbach," *IEEE Trans. Magn.*, vol. 57, no. 8, pp. 1-9, Aug. 2021.

[24] Z. Q. Zhu. "Electromagnetic performance of brushless permanent magnet dc motors with particular reference to noise and vibration," London, University of Sheffield, 1991.

Youyuan Ni was born in Anhui, China, in 1976. He received the B.Eng. and Ph.D. degrees in electrical engineering from Hefei University of Technology, Hefei, China, in 1999 and 2006, respectively. Since 2006, he has been with Hefei University of Technology, where he is currently an Associate Professor. His current research interests include design and control of electric machines.

Liang Zhang was born in Anhui, China, in 1996. He received the B.Eng. degree in electrical engineering and automation from the College of Electrical and Information Engineering of Hunan University of Technology, Hunan, China, in 2020. He is currently working toward the M.E. degree in electrical engineering with the School of Electrical Engineering and Automation, Hefei University of Technology. His current research interests include design of permanent magnet machines.

Zhiwei Qiu was born in Anhui, China, in 1996. He received the B.Eng. degree in mechanical engineering and automation from the College of Mechanical and Electrical Engineering of Anhui Jianzhu University, Anhui, China, in 2019. He is currently working toward the M.E. degree in electrical engineering with the School of Electrical Engineering and Automation, Hefei University of Technology. His current research interests include design of permanent magnet machines.